ACS SyntheticBiology

pubs.acs.org/synthbio Research Article

Rational Design of Novel Fluorescent Enzyme Biosensors for Direct Detection of Strigolactones

Rebecca J. Chesterfield, Jason H. Whitfield,* Benjamin Pouvreau, Da Cao, Kirill Alexandrov, Christine A. Beveridge, and Claudia E. Vickers

Cite This: *ACS Synth. Biol.* 2020, 9, 2107–2118 Read Online

ACCESS | Metrics & More | Article Recommendations | Supporting Information

ABSTRACT: Strigolactones are plant hormones and rhizosphere signaling molecules with key roles in plant development, mycorrhizal fungal symbioses, and plant parasitism. Currently, sensitive, specific, and high-throughput methods of detecting strigolactones are limited. Here, we developed genetically encoded fluorescent strigolactone biosensors based on the strigolactone receptors DAD2 from *Petunia hybrida*, and HTL7 from *Striga hermonthica*. The biosensors were constructed *via* domain insertion of circularly permuted GFP. The biosensors exhibited loss of cpGFP fluorescence *in vitro* upon treatment with the strigolactones 5-deoxystrigol and orobanchol, or the strigolactone analogue *rac*-GR24, and the ShHTL7 biosensor also responded to a specific antagonist. To overcome biosensor sensitivity to changes in expression level and protein degradation, an additional strigolactone-insensitive fluorophore, LSSmOrange, was included as an internal normalization control. Other plant hormones and karrikins resulted in no fluorescence change, demonstrating that the biosensors report on compounds that specifically bind the SL receptors. The DAD2 biosensor likewise responded to strigolactones in an *in vivo* protoplast system, and retained strigolactone hydrolysis activity. These biosensors have applications in high-throughput screening for agrochemical compounds, and may also have utility in understanding strigolactone mediated signaling in plants.

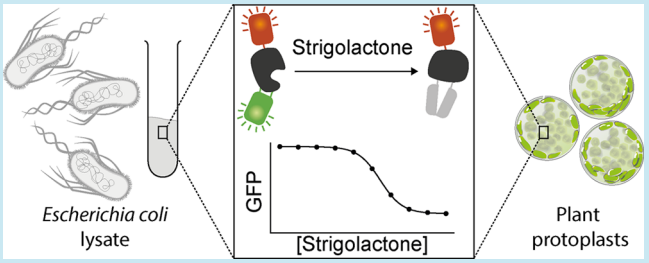

Strigolactones (SLs) are plant hormones involved in nutrient distribution, environmental adaptation, and plant development. They also function as rhizosphere signaling molecules in both symbiotic and parasitic interactions. Hormonal functions of strigolactones include branching inhibition, regulating root development and root hair growth, inhibiting adventitious rooting, increasing secondary growth, and promoting leaf senescence.[1−6] SLs have also been shown to improve plant survival and productivity under drought and salinity stress.[7−9] As rhizosphere signaling molecules, SLs induce hyphal branching in arbuscular mycorrhizae, promoting symbioses that are important for nutrient access in over 80% of land plant species.[10] However, SLs also trigger seed germination of *Striga* and *Orobanche spp.* of parasitic plants, and therefore play a major role in parasitization of crop plants.[11] These parasitic species infest upward of 60 million hectares of farmland worldwide, parasitizing most major cereal crops and leading to major economic burdens (losses reach $US billions annually) and food insecurity in endemic regions.[12]

The diverse functions of SLs (and SL-like compounds) lend themselves well to agricultural applications. A number of SL analogues have been investigated as *Striga* and *Orobanche* control agents (by inducing suicidal seed germination) with promising results.[13−15] SLs may also act as biofertilizers by enhancing mycorrhization, and their regulation of drought and salinity responses may provide the capacity to improve crop productivity under unfavorable conditions.[16] Furthermore, use of SLs to control plant architecture may contribute to the development of high-density, high-productivity planting systems, while crops with modified strigolactone production, composition, or perception show potential for improved agronomic properties.[17−20]

SLs are bound and hydrolyzed by the SL receptor D14 (known as DAD2 in petunia (*Petunia hybrida*)). This interaction induces a conformational change in D14 that triggers signal propagation (Figure 1).[21] SLs facilitate the interaction between D14, D3 (rice (*Oryza sativa*) nomenclature, known as MAX2 in other species), and D53 (or SMXL6/7/8 orthologues in *Arabidopsis* (*Arabidopsis thaliana*)) (Figure 1). D3 is the substrate-recognition F-box component of a Skp Cullin F-Box (SCF) E3 ubiquitin ligase complex, and D53 is a transcriptional repressor of SL signaling.[22] This interaction triggers ubiquitination and degradation of D53, mediating

Received: April 7, 2020
Published: July 28, 2020

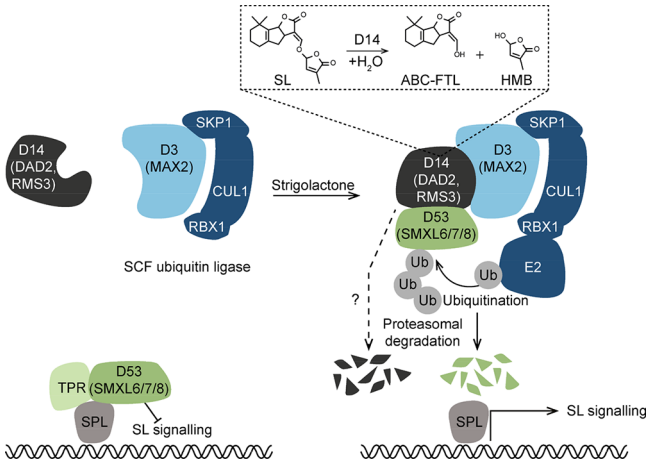

Figure 1. Strigolactone perception machinery. Schematic illustrating strigolactone signal propagation in plants. In the absence of SL, D53 (or SMXL6/7/8 orthologues) recruit TOPLESS-related (TPR) corepressors to repress SL signaling *via* transcription factors including Squamosa Promoter Binding Protein-like (SPL) family members. SL perception by D14 triggers interaction with D53 and D3, the substrate-recognition component of an SCF ubiquitin ligase complex. The SCF ligase ubiquitinates D53, targeting it for proteasomal degradation, and causing transcriptional derepression of SL signaling genes. D14 hydrolyses SLs, whether intact SL or a hydrolysis product trigger D14 conformational change and signal propagation is unresolved. SL signaling also results in D14/DAD2 degradation. Rice nomenclature is used, with alternative nomenclature shown in brackets. Figure adapted from ref 28. Copyright 2020, Cell Press.

downstream transcriptional changes.[23] SL signaling also induces degradation of D14[24,25] (Figure 1). D14 degradation is dependent on D3 and coupled to D53 degradation; however, it remains unknown whether D14 is a direct ubiquitination target of the SL-induced SCF complex, or is the target of a ubiquitin ligase expressed in response to D53 degradation.[25]

The biology and physiology of strigolactones is not yet fully elucidated, and there are indications that novel unidentified strigolactones exist.[26] A high-throughput detection method would facilitate their identification by allowing screening of a wide range of plant tissues and extracts. High-throughput detection would also simplify chemical library screening to identify strigolactone mimics with desirable agricultural properties, and accelerate metabolic engineering in microorganisms for development of strigolactone production platforms, which are of particular interest due to the difficulty of chemical synthesis.[16]

Currently, cost-effective, high-throughput methods for specific SL detection are limited. Strigolactones are typically detected and quantified by mass spectrometry, requiring expensive equipment and analytical standards. Functional assays, including parasitic seed germination and/or branching inhibition studies offer an alternative method of SL detection; however, accidental release of parasitic seeds is an environmental risk, and branching assays can be labor intensive. Differential scanning fluorimetry has also been successfully used to identify SL analogues and receptor antagonists by detecting the conformational changes of SL receptors.[27] Biosensors offer an alternative to existing assays with the potential for faster quantification of the target in the cellular and organismal context as well as the development of high-throughput screening tools.

In vivo SL biosensors have previously been developed by adapting the endogenous SL perception machinery. Making use of the SL-induced degradation of D53, Samodelov *et al.*[29] generated StrigoQuant, a D53-luciferase fusion that could detect SL signaling in *Arabidopsis* protoplasts. Similarly, Sanchez *et al.* generated transgenic *Arabidopsis* lines expressing a D14-luciferase fusion that could detect exogenously applied SLs and SL mimics by taking advantage of the endogenous feedback loop where SLs trigger degradation of D14.[30] Additionally, the SL-dependent interaction between DAD2 and MAX2 was initially demonstrated using a yeast two-hybrid (Y2H) system.[31] A similar Y2H approach enabled a high-throughput yeast screen for parasitic seed germination stimulants that relied on the interaction between MAX2 with HTL, a paralogue of *Arabidopsis* AtD14 that is involved in the perception of other plant signaling molecules, karrikins and cotylimides.[32] An analogous high-throughput yeast screen could conceivably be developed for SLs.

While the above-described multicomponent SL biosensors provided new tools for strigolactone research, the outputs of such systems may be difficult to interpret due to the nonquantitative nature of the reporter as well as the lag time between input and output. Moreover, given that multicomponent biosensors require integration of multiple signaling events, modulation of any individual component has potential to introduce noise or signaling artifacts. Direct quantitative detection of the target molecule would be ideal, however, design and construction of such biosensors is not straightforward owing to a lack of general design principles.[33]

In recent years, several methods for the development of integrated fluorescent sensors have emerged, aiming to allosterically link the fluorescent intensity of a circularly permuted green fluorescent protein (cpGFP) variant to the conformational state of a host receptor.[34−38] In circular permutation the N and C termini are connected *via* a short linker, while a new N and C are created elsewhere in the molecule. Positioning of new termini in proximity of the active center renders GFP highly sensitive to local conformational changes.[39] The conformational sensitivity of cpGFP can be exploited in biosensor design by inserting it into a molecular receptor with large ligand-dependent conformational transitions or by fusing two ligand binders to the new N and C termini. While highly successful, these approaches require significant and often library-based optimization of the variants to obtain biosensors with optimal sensitivity and dynamic range.[38] Ratiometric biosensors rely on a change in the fluorescence ratio between two emission wavelengths, rather than a fluorescence intensity change, and therefore are less dependent on biosensor concentration. This can be achieved by integrating an internal normalization control fluorophore into a cpGFP domain insertion biosensor.

In this work, we exploited structural and biophysical features of DAD2 and ShHTL7 enzymes to construct SL biosensors using cpGFP domain insertion. These were converted to ratiometric biosensors using LSSmOrange as an internal normalization control. While domain insertion biosensors have been developed using binding proteins and receptors for various ligands, to our knowledge, this is the first instance in which this cpGFP insertion strategy has been applied to an enzyme to monitor its enzymatic substrate. In addition to its utility for SL research this approach potentially significantly expands the type of protein modules that may be used for construction of protein biosensors.

https://dx.doi.org/10.1021/acssynbio.0c00192
ACS Synth. Biol. 2020, 9, 2107−2118

RESULTS AND DISCUSSION

Generation of an SL Biosensor by Fluorescent Protein Domain Insertion into DAD2. To develop an integrated SL biosensor, we applied the approach of fluorescent protein domain insertion into the petunia SL receptor, DAD2. Available crystal structures of the *Arabidopsis* DAD2 orthologue, AtD14, in *apo* and SL-induced conformations were used to guide the design process. DAD2 and AtD14 are composed of the catalytic domain and the lid domain, with the latter comprising α helices 5−8 (residues 136−194, Figure 2B, C).[31] For clarity, DAD2 numbering and secondary structure annotation (see ref 31) are used unless specified otherwise. The crystal structure of an SL-induced complex containing AtD14, rice D3, and ASK1, displays a large structural rearrangement of the AtD14 lid domain and the loop containing the catalytic Asp, compared to AtD14 *apo* structure (PDB codes 5HZG,[40] and 4IH4[41] respectively) (Figure 2B,C). We conjectured that this conformational transition in AtD14 can be induced by SLs in the absence of D3 and ASK1, and therefore used these structures to guide biosensor design.

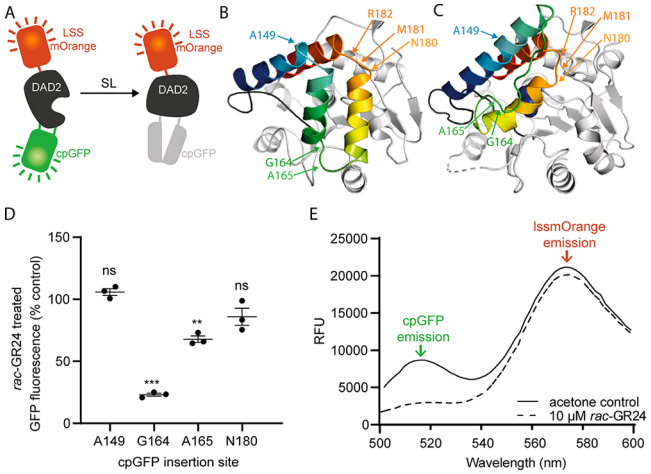

Figure 2. DAD2-based strigolactone cpGFP biosensor. (A) Schematic of the ratiometric DAD2 cPGFP biosensor design. Strigolactone-induced conformational change is propagated into cpGFP, modulating its fluorescence. The C-terminal LSSmOrange fusion provides an internal fluorescent control. (B) Structure of AtD14 in its apo conformation (PDB ID 4IH4), and (C) in a SL-induced complex containing AtD14, D3, and ASK1 (PDB ID 5HZG chain A). Density inside the binding pocket assigned to a hydrolysis product of the strigolactone analogue GR24 is shown in navy spheres. The lid domain is highlighted in rainbow and the Asp loop is shown in black. The six cpGFP insertion sites are indicated with arrows on each structure (DAD2 numbering), where the indicated residue is immediately N-terminal of the cpGFP insertion. (D) Fluorescent response of *E. coli* lysate expressing cpGFP-DAD2 chimers to 10 μM *rac*-GR24 at each insertion site. The data show the GFP fluorescence in *rac*-GR24 treated samples as a percentage of the fluorescence of the same variant under 0.1% acetone control conditions. Error bars represent standard error of the mean. *$p < 0.05$, **$p < 0.01$, ***$p < 0.001$ by one sample t test compared to theoretical mean of 100 (no difference). (E) Emission spectra of *E. coli* lysate expressing rDAD2 cPGFP(G164) in the presence or absence of 10 μM *rac*-GR24.

On the basis of structural analysis of AtD14 six DAD2 cPGFP insertion sites were selected: A149, G164, A165, N180, M181 and R182. A minimal linker of Ala-Ser was used to connect cpGFP to the target loop sites, as this appears sufficient to transduce minor loop rotations and perturbations in the host receptor[34] (Figure 2B,C).

Each domain insertion variant was expressed in *Escherichia coli*. The A149, G164, A165, and N180 variants expressed as partially soluble proteins, whereas the M181 and R182 variants were insoluble (Supporting Information, Figure S1). The cpGFP fluorescence of the A149, G164, A165, and N180 variants in *E. coli* lysate soluble fractions was measured in the presence or absence of the SL analogue *rac*-GR24. Insertion of cpGFP at two sites, G164 and A165 (both located between helices 6 and 7) exhibited reduced fluorescence in the presence of 10 μM *rac*-GR24, compared to a 0.1% acetone control (Figure 2D). The G164 variant denoted DAD2 cPGFP(G164) gave the largest change in fluorescence (Figure 2D, Supporting Information, Table S1). The SL-induced fluorescence change was also observed in live *E. coli* resuspended in phosphate buffered saline with or without *rac*-GR24 (Supporting Information, Figure S2). In contrast, insertions in the loops between helices 5 and 6, or helices 7 and 8, gave no significant change in fluorescence in response to *rac*-GR24 (Figure 2D). It is possible that insertion in these loops perturbed DAD2 structure, disrupting the interaction with *rac*-GR24 and loss of enzyme function. Alternatively, the insertions may not result in the propagation of conformational changes into cpGFP.

It should be noted that while the structural transition depicted in Figure 2B,C guided successful biosensor designs, it is unknown whether the conformation in Figure 2C is populated in the absence of D3, and therefore whether this rearrangement is responsible for the observed change in biosensor fluorescence. Indeed, fluorescence could instead be modulated by more subtle local structural changes in the flexible loop regions as is the case in similar conformationally sensitive sensor designs.[36,42] Understanding the events that the biosensor reports on is complicated by lack of consensus in the field surrounding the order of events involved in SL perception and signal transduction. Upon SL perception, SLs are hydrolyzed *via* a reaction that involves a hydrolysis intermediate covalently linked to the receptor, and DAD2 undergoes conformational change, facilitating interaction with the SCF ubiquitin ligase complex. However, it remains uncertain whether intact SL or a covalently linked hydrolysis product is responsible for triggering DAD2 conformational change and SCF complex formation. In the 5HZG AtD14-D3-ASK1 crystal structure, density inside the binding pocket was assigned to a D-ring derived molecule covalently linked to H247 and S97,[40] suggesting that this covalently linked intermediate molecule (CLIM) was the active form of SL (alternative reassignments of this density have since been suggested, as an iodide ion[43] or as a histidine-butenolide complex comprising the D-ring covalently bound to H247 only[21]). In contrast, AtD14 conformational change was found to correlate with GR24 concentration but not that of GR24 cleavage products posthydrolysis, and an enzymatically inactive mutant of AtD14 that could propagate SL signaling has been identified.[44] These latter findings support an alternative model in which uncleaved SL is the active form, with SL hydrolysis following signal propagation.

There is also lack of consensus regarding the longevity of the covalently linked hydrolysis intermediate(s). Using mass spectrometry, the peptide containing the histidine-butenolide complex of the SL D-ring bound to the catalytic histidine has been identified for AtD14, rice D14, the pea (*Pisum sativum*) orthologue RMS3, and the *Striga hermonthica* SL receptor

https://dx.doi.org/10.1021/acssynbio.0c00192
ACS Synth. Biol. 2020, 9, 2107−2118

ShHTL7.[40,45−47] Studies of RMS3 hydrolysis of a fluorescent substrate found that in the presence of excess substrate, RMS3 concentration limited the reaction progression with greater than a 1:1 RMS3:substrate ratio required to completely consume the substrate.[45] This result indicated that RMS3 acted as a single turnover enzyme, potentially due to irreversible formation of a histidine-butenolide complex. In contrast, a study using AtD14 found that GR24 was consumed over time at a 1:6 ratio of D14:GR24.[44] These contrasting results may reflect a difference in the stability of the hydrolysis intermediate between SL receptors in different species.

Despite ambiguity surrounding the molecular basis of fluorescence change, DAD2 cPGFP(G164) proved useful for SL detection, and was further developed. Intensiometric sensors that utilize only a single-fluorophore are effective as probes, but have limitations. In particular, intensiometric sensors are sensitive to changes in expression level and protein degradation, which are sources of significant noise for signal intensity. To rectify this, we sought to convert the biosensor to a ratiometric output that allows correction for those factors. This is achieved by adding a second fluorophore to provide an internal normalization control (Figure 2A). LSSmOrange has a long Stokes shift, allowing the cpGFP and LSSmOrange fluorophores to be excited by a single wavelength, while still providing spectrally resolved emission, as employed by the Matryoshka gCAMP sensors.[48] This approach exploits the nonoverlapping excitation−emission spectra of the fluorophores, eliminating confounding effects of FRET. LSSmOrange was fused at the C-terminus of the DAD2 cPGFP(G164) *via* a rigid GEAAAKEAAAKGG linker. The ratiometric sensor is denoted rDAD2 cPGFP(G164). Treatment of its solution with SL showed retention of the cpGFP intensity switching, while LSSmOrange fluorescence intensity was unaffected (Figure 2E), enabling calculation of a dose-dependent ratio change. The fluorescence ratio (cpGFP/LSSmOrange) decreased to 35% of its control value in the presence of 10 μM *rac*-GR24 (Figure 2E).

The DAD2 Conformational Biosensor Has High Sensitivity *in Vitro*. To test the sensitivity and detection range of rDAD2 cPGFP(G164) we initially measured the fluorescence ratio cpGFP/LSSmOrange in clarified *E. coli* lysate 10 min after adding various concentrations of *rac*-GR24. *rac*-GR24 had a detection range approximately between 50 nM and 500 nM, with an apparent EC50 of 143 ± 16 nM (Figure 3A).

As DAD2 is not only a receptor, but also an enzyme, we expected the biosensor fluorescence may change over time as it hydrolyzed the *rac*-GR24 substrate. We hypothesized that either fluorescence could return to control levels as *rac*-GR24 was consumed, or that a stable covalently bound reaction intermediate (a histidine-butenolide complex or CLIM) could stabilize the biosensor in the low-fluorescence conformation, and shift the biosensor pool toward the low-fluorescence state over time. A time course experiment showed the sensitivity of the biosensor increasing with incubation time (Figure 3A), consistent with the formation of a stable receptor-intermediate complex. Alternatively, it is possible that the kinetics of either *rac*-GR24 hydrolysis or the biosensor returning to a high-fluorescence state was too slow to see a return to control fluorescence over the time course examined.

In vitro, this time-dependent sensitivity may allow a larger detection range to be accessed simply by measuring at a range of time points. Additionally, sensitivity remained relatively

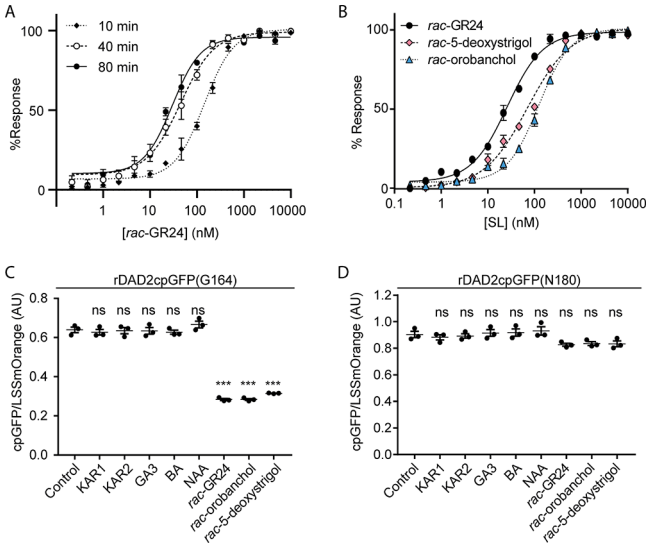

Figure 3. Analysis of sensitivity, specificity, and detection range of rDAD2 cPGFP(G164). (A) Dose−response curves of *E. coli* lysate of rDAD2 cPGFP(G164) after different incubation times with indicated concentrations of rac-GR24. (B) Dose−response curves of rDAD2 cPGFP(G164) to different SLs after 50 min incubation. (C) Fluorescent response of the rDAD2 cPGFP(G164) biosensor to SLs, but not other plant hormones or karrikins. (D) The rDAD2 cPGFP(N180) variant does not respond to SLs. KAR1 and KAR2: karrikins; GA3: gibberellic acid; BA: synthetic cytokinin 6-Benzylaminopurine; NAA: synthetic auxin 1-Naphthaleneacetic acid. Error bars represent standard error of the mean. Ns: not significant; ***$p < 0.001$ by Dunnett's multiple comparison test to the acetone control.

stable between 40 and 80 min, which permits a large number of samples to be processed and measured in parallel without significant influence from incubation time. In our system, we could detect *rac*-GR24 concentrations down to low nanomolar concentrations using a 40−80 min incubation time, with an apparent EC50 of 29.9 ± 4.7 nM at 80 min (Figure 3A).

Next, we investigated the response of the biosensor to the natural SLs 5-deoxystrigol and orobanchol, choosing 50 min incubation to ensure stable readings. The biosensor responded in a dose-responsive manner to both natural strigolactones tested (Figure 3B). The EC50 values were fit at 70.5 ± 6.3 nM for 5-deoxystrigol, and 124 ± 6.8 nM for orobanchol, which were significantly higher than that for *rac*-GR24 (EC50 = 25.9 ± 1.7 nM, extra sum-of-squares F test, $p < 0.0001$). The EC50 of *rac*-GR24 was also measured using purified DAD2 cPGFP(G164), and gave a similar value to the lysate samples (EC50 = 21.3 ± 1.7 nM after 50 min incubation) (Supporting Information, Figure S3). In contrast, the biosensor did not respond to karrikins KAR1 or KAR2, which bind a receptor related to DAD2, or other phytohormones, gibberellic acid (GA3), synthetic cytokinin 6-benzylaminopurine (BA), or synthetic auxin 1-naphthaleneacetic acid (NAA) (Figure 3C). Thus, rDAD2 cPGFP(G164) responded specifically to compounds known to bind the SL receptor. The non-responsive control variant rDAD2 cPGFP(N180) demonstrated that the fluorescence changes could not be accounted for by the fluorophores themselves, and were dependent on their insertion into a conformationally sensitive location of DAD2 (Figure 3D).

This sensitivity is on par with current mass spectrometry limits of detection: a recent SL quantification method

https://dx.doi.org/10.1021/acssynbio.0c00192
ACS Synth. Biol. 2020, 9, 2107−2118

development paper reported a limit of detection of 4.94 μg/L (16.6 nM) for *rac*-GR24.[49] Furthermore, the sensor does not require specialized equipment, and is adaptable to high-throughput applications. Unlike mass spectrometry, the biosensor cannot identify specific strigolactones; however, it distinguished strigolactones from karrikins and other hormones. In this respect, the biosensor could be used as a simple and scalable alternative to existing functional assays, such as branching inhibition bioassays, for some research applications.

A Gene Expression SL Biosensor Has Lower Sensitivity than rDAD2 cPGFP(G164). For many applications, transcriptional biosensors and transcription-independent protein biosensors are the two major blueprints for biosensor design for small molecule detection. In this context, we initially developed a yeast two-hybrid (Y2H)-based transcriptional biosensor in parallel to rDAD2 cPGFP(G164). The Y2H reporter was similar to a design reported by Hamiaux *et al.*,[31] but with different activation and binding domains. By fusing DAD2 to a DNA binding domain and MAX2 to an activation domain, transcription of the reporter gene (yEGFP) in *Saccharomyces cerevisiae* was coupled to SL-dependent interaction between DAD2 and MAX2 (Supporting Information, Figure S4A). After 16 h incubation with *rac*-GR24, the Y2H biosensor exhibited GFP fluorescence at low micromolar concentrations of *rac*-GR24 (Supporting Information, Figure S4B). This was much lower sensitivity than the conformational biosensor, potentially due to poor uptake of *rac*-GR24 by the cells, or alternatively due to minimum concentration requirements of the reconstituted transcription factor. Similarly, while the Y2H reporter developed by Hamiaux *et al.* had higher sensitivity than that developed here, the EC50 was approximately 10 times higher than that observed for the direct-detection domain insertion biosensor.[31] As the Y2H approach had lower sensitivity, slower response times, and was restricted to use in a single organism, the domain insertion biosensor was pursued for further applications.

The DAD2 Conformational Biosensor Detects SL in Protoplasts. Plant protoplasts can be used as a cell-based model for plant systems, providing a simple system for transient expression of proteins of interest. Accordingly, protoplasts have been used extensively in studies of strigolactone signaling.[25,29,50−52] We therefore chose protoplasts as a model system for proof of concept of the DAD2 conformational biosensor function in plant cells.

Tobacco protoplasts transfected with rDAD2 cPGFP(G164) were examined by flow cytometry, and exhibited fluorescence in GFP and LSSmOrange channels. Upon treatment with *rac*-GR24, GFP fluorescence decreased to just above background, whereas LSSmOrange fluorescence decreased only slightly, likely due to loss of bleed-through from cpGFP (Figure 4A,B). As GFP fusions of rice OsD14 and *Arabidopsis* AtD14 are degraded *in vivo* 2−24 h after treatment with GR24,[24,25] LSSmOrange fluorescence was examined at longer time points for evidence of protein degradation. After the initial slight decrease attributed to loss of bleed-through from cpGFP, no further fluorescence change was observed up to 24 h, suggesting that rDAD2 cPGFP(G164) was not degraded in response to *rac*-GR24 (Figure 4B). It is possible that the cpGFP insertion may prevent interactions required for ubiquitination.

The cpGFP/LSSmOrange fluorescence ratio changed in response to *rac*-GR24 in a dose-dependent manner. As observed *in vitro* in bacterial lysates, there was a slight time-dependent response: the apparent EC50 was 205.4 nM after 30 min, and decreased to 119.3 nM after 60 min (Figure 4C).

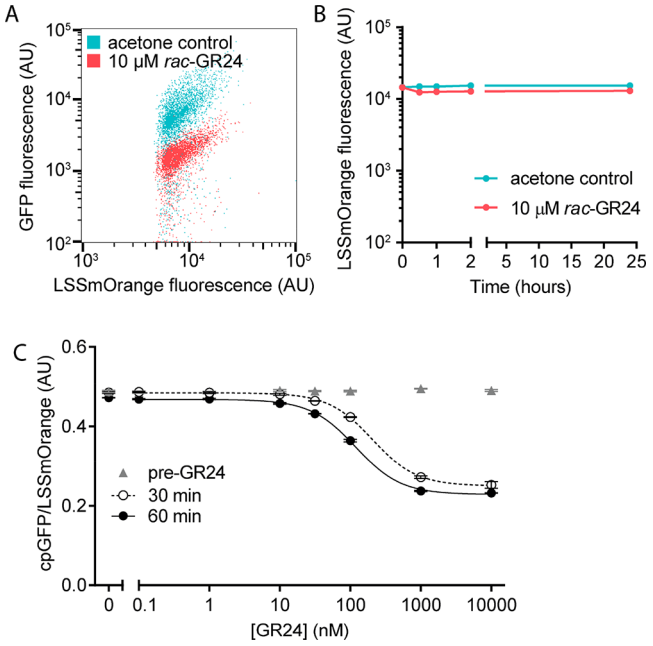

Figure 4. rDAD2 cPGFP(G164) responds to *rac*-GR24 in protoplasts. (A) Dot plot of protoplasts expressing rDAD2 cPGFP(G164) 1 h after treatment with 10 μM *rac*-GR24 or acetone control. For clarity, only cells gated for positive LSSmOrange fluorescence are shown. (B) LSSmOrange fluorescence of protoplasts expressing rDAD2 cPGFP(G164) treated with 10 μM *rac*-GR24 or acetone control plotted as a function of time over 24 h. (C) Dose−response curve of protoplasts transformed with rDAD2 cPGFP(G164) to *rac*-GR24. Each sample was measured prior to, 30 min after, and 60 min after addition of *rac*-GR24, and data represent mean cpGFP fluorescence of all live cells normalized to mean LSSmOrange fluorescence. Data show mean ± standard error of three replicates.

The functionality of rDAD2 cPGFP(G164) in tobacco protoplasts demonstrates proof-of-concept for application of this biosensor in signaling studies. In this respect, it is likely to complement existing biosensors for dissecting aspects of SL signal transduction. Existing SL biosensors report on degradation of D14 or D53,[29,30] and as such, are dependent on many cellular processes, including the activity of additional signaling components, proteasomal degradation, and in the case of the D14-based biosensor, on unknown processes that may involve gene transcription. As the only direct-detection biosensor developed to-date, the DAD2 conformational biosensor provides new potential for detecting SLs in plants and unravelling the processes that contribute to SL signaling.

Considerable differences in sensitivity were seen across the strigolactone biosensors developed to-date. StrigoQuant, which reported on D53 degradation, had very high sensitivity, detecting 5-deoxystrigol at concentrations as low as 100 fM, and orobanchol down to 10 nM.[29] In contrast, the D14 degradation-based *in planta* bioassay had an EC50 of 1.63 μM GR24.[30] The conformational biosensor developed here had intermediate sensitivity, with EC50s in the low- to mid-nanomolar range, while transcriptional Y2H-based biosensors had lower sensitivity. These differences may be expected due to the differing reliance of each biosensor on additional cellular processes. For example, in the StrigoQuant system, ubiquitination of multiple luciferase-tagged D53 molecules by a single

https://dx.doi.org/10.1021/acssynbio.0c00192
ACS Synth. Biol. 2020, 9, 2107−2118

SL-induced SCF E3 ligase complex may mediate signal amplification. Conversely, the uncharacterized signaling steps between SL binding and D14 degradation may dampen signal. In addition, differences in the sensitivity of the parent receptors used, and changes induced through modification for biosensor construction, likely impact SL binding affinity.

The DAD2 Conformational Biosensor Retains Catalytic Activity. Ideally, the DAD2 conformational biosensors would retain SL binding and hydrolysis activities similar to the wild-type receptor, thus enabling a close to native condition direct-detection method. To test enzymatic activity of DAD2 cPGFP(G164), hexahistidine tagged wild-type DAD2 and DAD2 cPGFP(G164) were purified (Supporting Information, Figure S5), incubated with *rac*-GR24, and both *rac*-GR24 and a hydrolysis product, ABC-FTL, were monitored by LC-MS/MS (Figure 5A). The *rac*-GR24 peak intensity decreased in

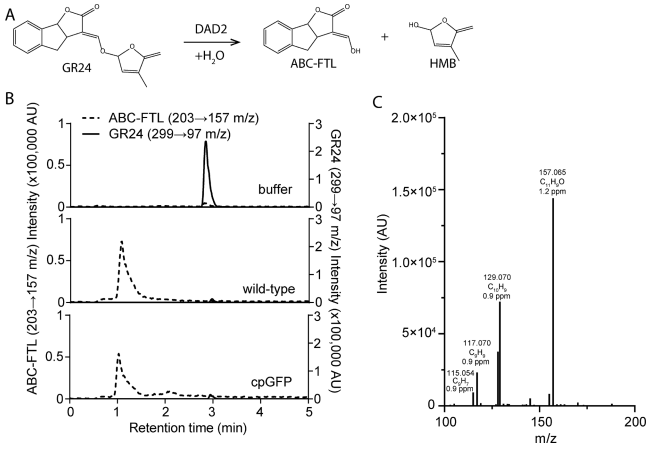

Figure 5. DAD2 cPGFP(G164) hydrolysis activity toward *rac*-GR24. (A) DAD2 hydrolyses GR24 to produce two products, ABC-FTL and HMB. (B) Extracted ion chromatograms showing hydrolysis of *rac*-GR24 (299 → 97 m/z transition, 3.0 min retention time) by purified wild-type DAD2 and DAD2 cPGFP(G164) to form ABC-FTL (203 → 157 m/z transition, 0.6 min retention time). Data show representative peak from three replicate samples. (C) MS2 Product ion scan of the 203.07 m/z peak analyzed on an Orbitrap Elite mass spectrometer.

samples incubated with wild type DAD2 or DAD2 cPGFP-(G164) compared to a buffer-only control, and a new peak consistent with the fragmentation pattern of ABC-FTL[31] appeared (Figure 5B). To confirm the identity of ABC-FTL, accurate mass was confirmed to within 1 ppm for both DAD2 and DAD2 cPGFP(G164) samples, and the fragmentation pattern matched that published previously[31] (Figure 5C).

The enzymatic activity of DAD2 toward SL makes it unique as a biosensor recognition domain. Receptors, and more broadly small molecule binding proteins such as calmodulin and periplasmic binding proteins, have been widely used as biosensor components.[34−37] In contrast, enzymes have been largely overlooked as input domains. To our knowledge, where domain insertion enzyme biosensors have been developed previously, they have reported on enzyme conformation or nonsubstrate ligands, but have not been used to detect their substrate.

There are several potential reasons for which enzymes may have traditionally been overlooked as biosensor input domains. First, enzymes can have comparatively small conformational change upon substrate binding compared to receptors. However, it is becoming clear that small conformational changes can induce signal output. Second, the temporary nature of substrate binding during enzyme catalysis could generate a transient signal that may be difficult to detect. Yet we found that signal from the DAD2 enzyme biosensor persisted sufficiently to measure fluorescence change even at low substrate concentrations. This work demonstrates the utility of enzymes as biosensors for their substrate, which provides a precedent that may expedite the development of new biosensors. Previously, development of biosensors for new analytes relied on scouring databases for potential binding proteins or mutating known binding proteins to change their ligand specificity. As many potential analytes are substrates for known enzymes, these enzymes significantly broaden the pool of characterized proteins from which we can draw input domains for biosensor development.

Generation of an SL Biosensor by Fluorescent Protein Domain Insertion into ShHTL7. The different activities of SLs as hormones, parasitic seed germination stimulants, and mycorrhizae communication molecules are mediated by different receptors.[53] In model plants, SLs are detected by D14/DAD2, whereas seed germination of the parasitic *Striga hermonthica* is mediated by a related clade of α/β hydrolases that underwent convergent evolution to recognize SLs.[54] The *S. hermonthica* HTL7 (ShHTL7) is the most sensitive of these receptors, and plays a dominant role in *S. hermonthica* seed germination.[55] An expected challenge in using SLs for agricultural applications is the risk of unintended activities arising from the diverse functions of SLs in hormonal, symbiotic and parasitic signaling. Increasing the specificity of the compounds toward one receptor type would reduce off-target effects. We asked whether we could apply the same principle used for DAD2 cPGFP(G164) to generate an ShHTL7-based SL biosensor with the goal of being able to differentially detect the propensity of an SL analogue to activate hormonal and parasitic seed germination pathways.

To rationally design an ShHTL7 version of the SL biosensor using DAD2 cPGFP(G164) as a template, we aligned structures of ShHTL7 and DAD2 (PDB ID 5Z7Y[56] and 4DNP,[31] respectively). The two receptors have conserved global tertiary structure (Figure 6A). We therefore hypothesized that domain insertion into the loop between helices 6 and 7 of ShHTL7 may facilitate coupling of SL-binding and cpGFP fluorescence, as observed in DAD2 cPGFP(G164). Insertion of cpGFP was tested at four loop positions between helices 6 and 7, with LSSmOrange fused to the C terminus to enable ratiometric measurement. Insertion after L166 displayed sensitivity to SL-binding, with greater than 2-fold reduction in cpGFP fluorescence in the presence of 10 μM *rac*-GR24, and dose-responsive behavior toward *rac*-GR24 (EC50 = 8.9 ± 0.7 nM), *rac*-5-deoxystrigol (EC50 = 115.5 ± 15.9 nM) and *rac*-orobanchol (EC50 = 34.9 ± 2.7 nM) (Figure 6B, C, Supporting Information, Table S1). In contrast, rShHTL7 cPGFP(L166) did not respond to karrikins, or the phytohormones GA3, BA, or NAA (Figure 6D). On the basis of sequence alignment, L166 is equivalent to DAD2 V167, not G164 (Figure 6A), which highlights the importance of testing multiple insertion sites. Nevertheless, this suggests that in some cases, paralogous proteins can be successfully used as guides to direct sensor design, although this is not generalizable to all protein scaffolds.[57]

Triton X-100 specifically binds and inhibits ShHTL7 but does not inhibit rice and *Arabidopsis* D14 orthologues of

https://dx.doi.org/10.1021/acssynbio.0c00192
ACS Synth. Biol. 2020, 9, 2107−2118

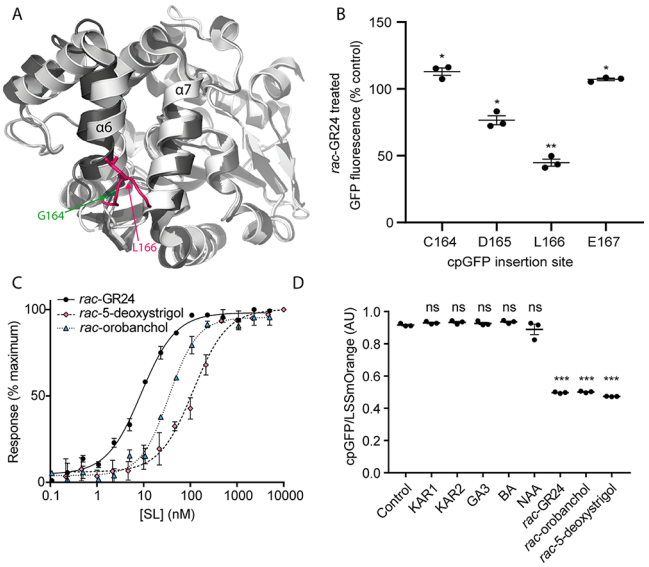

Figure 6. Characterization of the SL sensing cpGFP-ShHTL7 chimera. (A) Alignment of DAD2 (PDB ID 4DNP; light gray) and ShHTL7 (PDB ID 5Z7Y; dark gray). DAD2 G164 is highlighted in green and ShHTL7 cPGFP insertion sites between helices 6 and 7 are highlighted in pink, with the ShHTL7 L166 side chain shown. (B) Fluorescent response to the strigolactone analogue *rac*-GR24 (10 μM) at each insertion site. The data show the GFP fluorescence in *rac*-GR24 treated samples as a percentage of the fluorescence of the same variant under 0.1% acetone control conditions. ANOVA test for equality of means $p < 0.0001$; $^{*}p < 0.05$, $^{**}p < 0.01$, one sample *t* test compared to theoretical mean of 100 (no difference). (C) Dose–response curve of rShHTL7 cPGFP(L166) incubated with *rac*-GR24, *rac*-5-deoxystrigol and *rac*-orobanchol after 50 min incubation. (D) Fluorescent response of the rShHTL7 cPGFP(L166) biosensor to SLs, but not other plant hormones or karrikins. KAR1 and KAR2: karrikins; GA3: gibberellic acid; BA: synthetic cytokinin 6-benzylaminopurine; NAA: synthetic auxin 1-naphthaleneacetic acid. Error bars represent standard error of the mean. Ns: not significant; $^{***}p < 0.001$ by Dunnett's multiple comparison test to the acetone control. All error bars represent standard error of the mean of three replicates.

DAD2.[55] Structural and mutagenesis studies indicated that the inability of D14 to bind Triton X-100 was due to a leucine to alanine substitution at ShHTL7 L143, which prevents a widening of binding pocket required for Triton X-100 binding.[55] As DAD2 has phenylalanine at this position, it is not expected to interact with Triton X-100. When Triton X-100 was preincubated with rDAD2 cPGFP(G164) for 2 h, it had no effect on the control lysate, and did not prevent *rac*-GR24-induced loss of cpGFP fluorescence (Supporting Information, Figure S6, Table S1). In contrast, Triton X-100 reduced the cpGFP fluorescence of rShHTL7 cPGFP(L166), and no further change was observed upon *rac*-GR24 treatment. ShHTL7 undergoes only minor conformational change upon Triton X-100 binding.[55] Therefore, these results suggest that the cpGFP is sensitive to small local conformational changes, and rShHTL7 cPGFP(L166) appears to report on agonist and antagonists similarly.

The DAD2 and ShHTL7 biosensors may offer a new method to identify SL mimics with increased specificity toward DAD2 and/or ShHTL7. Indeed, biosensors have demonstrated utility in drug discovery screens due to their high specificity and affinity, and integrated output module. In a similar way, the SL biosensors developed here could be used for screening small molecule libraries for agonists or antagonists of DAD2 and/or ShHTL7, with the ability to distinguish binding to each receptor. Compounds with targeted hormonal or seed germination activity are already being identified as promising leads for agrochemical development,[27,58] and the application of these biosensors may expedite similar studies.

The two new high-sensitivity biosensors developed here are a valuable addition to the SL detection toolbox. As these are the first biosensor designs, there is much scope to improve signal dynamic range *via* linker engineering and optimization of fluorescent proteins. The sensors provide a direct method of detection and quantitation for SLs, with low nanomolar sensitivity, and have particular value in any high-throughput applications. Combined, the DAD2 and ShHTL7 biosensors offer new capability to distinguish the ability of a SL mimic to bind the hormonal receptor from its binding to the parasitic seed germination receptor. Therefore, the sensors have potential applications in screening compound libraries for potential agrochemicals. Compared to existing biosensors, the direct-detection biosensors developed here offer simplicity, versatility across multiple organisms and *in vitro* systems, and reduced risk of confounding effects from other signaling components. The application of enzymes as biosensor recognition modules for their substrates sets a new precedent in biosensor design, and this approach is expected to have applications in developing new biosensors.

METHODS

Plasmid Construction. DAD2, ShHTL7, cpGFP and LSSmOrange were codon optimized and synthesized as gene fragments, where DAD2 was synthesized in fusion to LexA DNA binding domain for use in the Y2H-based sensor (Integrated DNA Technologies; Supporting Information, Table S2). All primers are listed in Supporting Information, Table S3, and all PCR amplifications used Phusion high-fidelity polymerase (NEB) or PrimeStarGXL polymerase (Takara) as per the manufacturers' protocols.

DAD2 cPGFP variants were constructed by amplifying variable N- and C-terminal portions of each receptor, and assembling with the cpGFP fragment into pET19b between BlpI and NcoI using Gibson assembly (NEB). N-terminal portions were amplified using primer DAD2N-F1 and a variable reverse primer, whereas C-terminal portions were amplified using a variable forward primer and DAD2C-R1. The plasmid encoding DAD2 cPGFP(G164) was denoted pET19b-DAD2 cPGFP(G164). To generate pET19b-rDAD2 cPGFP-(G164), encoding the ratiometric DAD2 biosensor, the LSSmOrange coding sequence was amplified using LSSmOrange-F and LSSmOrange-R primers and DAD2C-R2 was used as the reverse primer for the C-terminal portion to confer homology to LSSmOrange. pET19b-rDAD2 cPGFP(G164) was constructed by Gibson assembly of N- and C-terminal portions of DAD2, cpGFP, and LSSmOrange into pET19b between BlpI and NcoI sites.

For ShHTL7 constructs, a base plasmid was initially constructed by assembling the ShHTL7 gene fragment with the LSSmOrange amplicon (LSSmOrange-F and LSSmOrange-R primers) into pET19b between BlpI and NcoI sites. The entire base plasmid was then amplified to introduce homologous ends to cpGFP at each insertion location using different primer sets (Supporting Information, Table S3), and the amplicons were assembled with the cpGFP gene fragment

https://dx.doi.org/10.1021/acssynbio.0c00192
ACS Synth. Biol. 2020, 9, 2107–2118

using Gibson cloning (NEB). The plasmid encoding rShHTL7 cPGFP(L166) was denoted pET19b- rShHTL7 cPGFP-(L166).

6His-DAD2 and 6His-DAD2 cPGFP(G164) were amplified from the DAD2 gene fragment and pET19b-DAD2 cPGFP-(G164), respectively, using primers DAD2N-F2 (1/10000 dilution of standard primer concentration), DAD2N-F3 and DAD2C-R1, where DAD2N-F3 anneals to the 5′ end of DAD2N-F2. This allowed initial amplification of the template by DAD2N-F2, followed by subsequent amplification by DAD2N-F3. Amplicons were cloned by Gibson assembly (NEB) into pET19b between BlpI and NcoI sites, generating pET19b-HisDAD2 and pET19b-HisDAD2 cPGFP(G164).

For protoplast experiments, rDAD2 cPGFP(G164) was amplified using primers 441 and 442, then digested with ClaI and SpeI and ligated into the minimal protoplast vector developed by Pouvreau *et al.*[59]

pY2H-GFP was constructed by homologous recombination *in vivo* assembly in CEN.PK2−1C. Homologous arms for recombination at the YARCΔ8 locus were PCR amplified from CEN.PK113−7D genomic DNA using primers 101 + 102 for the upstream arm, and primers 122 + 123 for the downstream arm. PGAL1 and PGAL2 promoters and TIDP1T, TLCS2 and TRPL41B terminators were PCR amplified from CEN.PK113−7D genomic DNA using the following primer pairs: 103 + 104, 33 + 108, 107 + 32, 111 + 112, and 120 + 121 respectively. The GFP coding sequence was amplified from plasmid pILGFP3 (Addgene 65451) using primers 117 + 118. Coding sequences of a fusion of DAD2 to the LexA DNA binding domain (LexA-DAD2), and of MAX2 to the B42 activation domain (B42AD-MAX2) were synthesized as gene fragments (Integrated DNA Technologies). A synthetic promoter (PLexA) consisting of eight repeats of the LexA operator and a minimal GAL1 promoter was also synthesized (GenScript). LexA-DAD2, B42AD-MAX2 and PLexA were PCR amplified using primers 105 + 106, 109 + 110, and 113 + 124, respectively. All PCR fragments were purified using EasyPure PCR Purification Kit (TransGen Biotech) as per the manufacturer's protocol and cotransformed into CEN.PK2−1C with pRS425 episomal plasmid backbone digested with SfoI and SacI (NEB). The assembled plasmid was extracted from *S. cerevisiae*, propagated in *E. coli*, and verified by sequencing. Next, pY2H-GFP was adapted to include a URA3 selection marker to produce pY2H-GFP(URA3). GFP-TRPL41B and the downstream YARCΔ8 homologous recombination are were PCR amplified from pY2H-GFP with primers 183 + 184 and 187 + 188, respectively. The URA3 selection marker was PCR amplified from pRS426 with primers 185 + 186. The resulting PCR fragments were reassembled into pY2H-GFP digested with BssHII and NdeI using Gibson cloning (NEB) and confirmed by sequencing. The verified plasmid was digested with SwaI and transformed into CEN.PK2−1C for genomic integration at the YARCΔ8 locus, producing yeast strain ScY2H-GFP(URA3).

Chemicals. *Rac*-GR24 was a gift from Christopher S. P. McErlean (The University of Sydney). *Rac*-orobanchol and *rac*-5-deoxystrigol were purchase from Chiralix. Gibberellic acid (GA3), 6-benzylaminopurine (BA), and 1-naphthaleneacetic acid (NAA) were from Sigma. KAR1 and KAR2 were a gift from Gavin Flematti (University of Western Australia).

Domain Insertion Screen: Immunoblotting and *rac*-GR24 Response. *E. coli* Rosetta (DE3) (DAD2 constructs) or BL21 (DE3) containing pGro7 (Takara) (ShHTL7 constructs) were used for recombinant protein expression. Fresh LB medium (10 mL) containing 100 μg/mL ampicillin and 34 μg/mL chloramphenicol was inoculated with overnight precultures and grown at 37 °C, 200 rpm until $0.5 < OD_{600nm} < 1.0$. Cultures were induced with 1 mM IPTG then incubated for 16−20 h at 20 °C, 200 rpm. Two mL aliquots of culture were centrifuged and *E. coli* were stored as pellets at −30 °C until use. *E. coli* were lysed by sonication (3 × 15 s at 30% power) in 600 μL 50 mM Tris-HCl, 150 mM NaCl (pH 7.5) supplemented with 1 mg/mL lysozyme, 1 mM DTT and 1 × EDTA-free protease inhibitor cocktail (Roche). Lysates were clarified by centrifugation at 17 000*g*, 4 °C for 10 min.

For immunoblotting, soluble and insoluble fractions were separated, and the insoluble fraction was resuspended in an equal volume (600 μL) of lysis buffer. Samples were separated by SDS-PAGE using Mini-PROTEAN TGX precast gels, then transferred onto poly(vinylidene fluoride) membranes using the Trans-Blot Turbo Transfer System (BioRad). Membranes were blocked in phosphate buffered saline (PBS) with 0.1% TWEEN 20 and 5% skim milk powder overnight, then incubated with mouse α-GFP primary antibody (Cell Signaling catalogue number 2955S) diluted 1/2000 into blocking buffer for 2 h at room temperature. Membranes were washed in PBS with 0.1% TWEEN 20 three times over 15 min, then incubated for 1 h with horse radish peroxidase-conjugated α-mouse IgG secondary antibody (Cell Signaling catalogue number 7076P2) diluted 1/1000 in PBS with 0.1% TWEEN 20. After washing, immunoblots were imaged using Clarity Western ECL substrate as per the manufacturer's protocol, using a ChemiDoc XRS+ system (BioRad). Replicate SDS-PAGE gels were run, and stained using GelCode blue safe protein stain (ThermoFisher Scientific) to assess loading.

To assess *rac*-GR24 response, 200 μL lysate soluble fraction was transferred to a microtiter plate containing *rac*-GR24 or a solvent-only (acetone) control to a final concentration of 0.1% acetone with or without 10 μM *rac*-GR24. Fluorescence was measured using a Tecan Infinite 200 Pro microplate reader at 465 nm excitation, 517 nm emission (GFP), and 465 nm excitation, 575 nm emission (LSSmOrange). For analysis of intact *E. coli*, 2 mL aliquots of fresh culture were centrifuged and *E. coli* were resuspended in 600 μL phosphate buffered saline, then 200 μL cell suspension was transferred to a microtiter plate containing *rac*-GR24 or a solvent-only control to a final concentration of 0.1% acetone ±10 μM *rac*-GR24, and fluorescence was measured as per the lysate assay.

Protein Purification. 6His-DAD2 and 6His-DAD2 cPGFP(G164) were expressed as per the domain insertion screen, except 800 mL cultures were used, and expression was induced with 400 μM IPTG. *E. coli* were lysed in 10 mM HEPES-NaOH, 150 mM NaCl (pH 7.5) by passing twice trough an Emulsiflex C5 high pressure homogenizer (Avestin) at 15 000 psi, then clarified by centrifugation at 18 000*g* 4 °C for 30 min. Supernatants were filtered through 0.22 μm poly(ether sulfone) Millex-GP syringe filters, then supplemented to a final concentration 20 mM imidazole. Each protein was purified using a 1 mL HisTrap HP column (GE Healthcare), washing with 10 mM HEPES-NaOH, 150 mM NaCl, 20 mM imidazole (pH 7.5) and eluting with 10 mM HEPES-NaOH, 150 mM NaCl, 200 mM imidazole (pH 7.5). Protein concentration was quantified using a NanoDrop, and adjusted for purity as determined by SDS-PAGE.

Dose−Response Curves. Lysates expressing rDAD2 cPGFP(G164) or rShHTL7 cPGFP(L166) were prepared as

https://dx.doi.org/10.1021/acssynbio.0c00192
ACS Synth. Biol. 2020, 9, 2107−2118

per the domain insertion screen, with the exception that lysates were further diluted to a final volume of 3−10 mL lysate from 2 mL culture. For dose−response curves using lysate, 90 μL supernatant was transferred to a microtiter plate, followed by 10 μL of 2.15 nM to 100 μM SL serial dilutions in 50 mM Tris-HCl, 150 mM NaCl, 1% acetone (pH 7.5) to final concentrations of 215 pM to 10 μM SL, 0.1% acetone after addition to lysate. Fluorescence was measured at indicating time points using a Tecan Infinite 200 Pro microplate reader as per the domain insertion screen. Dose−response curves using purified 6His-DAD2 cPGFP(G164) were performed in 200 μL 50 mM Tris-HCl, 150 mM NaCl at final concentrations of 6 nM protein with 215 pM to 10 μM SL and 0.1% acetone. Fluorescence was measured using a Tecan Infinite 200 Pro microplate reader at 480 nm excitation, 517 nm emission.

Strigolactone, Karrikin, Other Phytohormone, and Triton X-100 Treatments. Lysates were prepared as per dose−response curves. Ten μL KAR1, KAR2, GA3, BA, NAA, *rac*-GR24, *rac*-orobanchol, and *rac*-5-deoxystrigol were incubated with clarified lysates expressing rDAD2 cPGFP(G164), rDAD2 cPGFP(N180) and rShHTL7 cPGFP(L166) at a final concentration of 0.1% acetone for 10 min prior to fluorescence measurements. For Triton X-100 analyses, clarified lysates were incubated for 2 h on ice with or without 100 μM Triton X-100, then treated with 10 μM *rac*-GR24 or acetone control and fluorescence was measured immediately. Fluorescence was measured using a Tecan Infinite 200 Pro microplate reader as per the domain insertion screen.

Yeast Cell Culture and *rac*-GR24 Treatment of Yeast Biosensor. During strain construction and all precultures, yeast strains were grown on YPD, or where auxotrophic selection was required, on 6.7 g/L yeast nitrogen base without amino acids (YNB) supplemented with 20 g/L glucose. YNB pH was adjusted to 6.0 with ammonium hydroxide, and YNB was supplemented with 20 mg/L histidine, 100 mg/L leucine and 100 mg/L tryptophan (ScY2H-GFP(URA3)), and with 20 mg/L uracil for the CEN.PK2−1C control. For cultivation on Petri dishes, media were solidified with 20 g/L bacteriological agar.

For *rac*-GR24 treatment experiments, ScY2H-GFP(URA3) yeast were streaked from glycerol stocks onto YNB agar and grown for 2 days at 30 °C. Single colonies were inoculated into a primary preculture in 5 mL YNB in McCartney bottles and grown for 24 h. A secondary preculture (5 mL YNB in a McCartney bottle) was inoculated from the primary preculture using a volume of culture such that the secondary preculture would reach mid log phase the following morning (based on cell density and preliminary growth rate estimates). Experimental cultures were inoculated from secondary precultures to a starting culture density of OD_{600nm} = 0.2 into 100 mL shake flasks containing 5 mL YNB MES + medium (6.7 g/L YNB without amino acids, 100 mM MES pH 6.0, 100 mg/L glutamic acid, 120 mg/L lysine, 40 mg/L methionine, 50 mg/L phenylalanine, 375 mg/L serine, 200 mg/L threonine, and 10 mg/L myo-inositol) supplemented with 2% galactose, 35 mg/L histidine, 110 mg/L leucine, 100 mg/L tryptophan, and 40 mg/L uracil (CEN.PK2−1C only), with or without 10 μM *rac*-GR24. Strains were cultured for 16 h at 30 °C, 200 rpm, then GFP fluorescence was measured by flow cytometry (BD Accuri C6; BD Biosciences, USA) using a 488 nm laser and 530/20 nm band-pass filter. The dose−response curves were performed as described with the exception that experimental cultures were in 1 mL medium, in 6-well plates.

GR24 Hydrolysis Assays. Thirty μM 6His-DAD2, 6His-DAD2 cPGFP(G164) or a buffer-only control was incubated with 30 μM *rac*-GR24 in 10 mM HEPES-NaOH, 150 mM NaCl pH 7.5 in 50 μL reaction volumes at 30 °C for 2 h. *rac*-GR24 and reaction products were extracted twice into 50 μL ethyl acetate. The extract was diluted with 100 μL acetonitrile then vacuum centrifuged to 30 μL. Two μL of each extraction was analyzed by LC-MS/MS. The LC-MS system was a Nexera X2 ultra high pressure liquid chromatograph (UHPLC) system (Shimadzu Corporation, Kyoto, Japan) coupled with a 5500 QTRAP MS system equipped with an electrospray ionization source (ESI) (AB Sciex, USA). SLs were separated on a Phenomenex Kinetex C18 reversed phase column (2.1 mm × 100 mm, 1.7 μm) maintained at 45 °C. The settings and gradients for UPLC are as follows: flow rate: 0.5 mL/min; mobile phase A: 0.1% acetic acid in deionized water; mobile phase B: 0.1% acetic acid in acetonitrile. The gradient was as follows: 30% to 100% B for 12 min, followed by 3 min wash with 100% B. MS/MS spectra were recorded using multiple reaction monitoring with the following settings: scan mode: positive; curtain gas: 20 psi; collision gas: high; ion spray voltage: 5500 V; ion source temperature: 500 °C; ion source gas 1:25 psi; ion source gas 2:25 psi. Declustering potential, entrance potential, collision energy and collision cell exit potential were set to 80, 10, 20, and 15 V, respectively.

Accurate mass and fragmentation patterns were confirmed as follows. Samples were separated using reversed-phase chromatography on a Dionex Ultimate 3000 RSLC nano-system. Using a flow rate of 30 μL/min, samples were desalted on a Thermo PepMap 100 C18 trap (0.3 × 5 mm, 5 μm) for 5 min, followed by separation on a Vydac Everest C18 column (150 mm × 75 μm, 5um particle) at a flow rate of 300 nL/min. A gradient of 10−50% buffer B over 7 min where buffer A = 1% ACN/0.1% FA and buffer B = 80% ACN/0.1% FA was used to separate molecules, followed by washing at 98% B for 3 min, before returning to 10% B. Eluted molecules were directly analyzed on an Orbitrap Elite mass spectrometer (Thermo) using an NSI electrospray interface. Source parameters included a capillary temperature of 275 °C; S-Lens RF level at 60%; source voltage of 2.4 kV and maximum injection times of 200 ms for MS and 150 ms for MS2. Instrument parameters included an FTMS scan across m/z range 50−500 at 60 000 resolution followed by information dependent acquisition of the top 10 singly charged peaks in the Orbitrap using HCD fragmentation, and normalized collision energy of 64 V. Dynamic ion exclusion was employed using a 15-s interval. Charge state screening was enabled with rejection of all ions other than +1 charged species.

Protoplast Preparation and Analysis. Tobacco protoplasts were prepared as per Pouvreau *et al.*[59] Flow cytometry analyses were conducted on an Invitrogen Attune NxT Flow Cytometer and analyzed with Invitrogen Attune NxT Software. Cells suspended in the protoplast buffer at a concentration of 0.187 M cells per ml were analyzed at a flow rate of 200 μL/min and data were acquired for 150 μL. Sample were complemented with propidium iodide (PI) at 1 μg/mL final concentration and incubated 15 min prior to Flow cytometric analyses. Chlorophyll and PI fluorescence were excited with a 561 nm laser and emissions were respectively captured by a 780/60 nm and a 620/15 nm band-pass filters. Protoplast population was gated based on SSC/FSC as well as Chlorophyll fluorescence/FSC ratios based on previous data (data not shown). Positive cells for PI staining (regarded as

https://dx.doi.org/10.1021/acssynbio.0c00192
ACS Synth. Biol. 2020, 9, 2107−2118

dead cells) were ignored for the rest of the analyses. For the remaining cells, LSSmOrange and cpGFP fluorescence were excited with a 488 nm laser and emissions were respectively captured by a 590/40 nm and a 530/30 nm band-pass filters. Unless otherwise stated, analyses were conducted on a minimum of three individual samples for each condition.

Each sample was run once through the flow cytometer and then immediately spiked 1:100 with GR4 in 10% acetone solution. Eight different final GR4 dilutions were used: 10 μM, 1 μM, 100 nM, 31.6 nM, 10 nM, 1 nM, 0.1 nM, and 0 nM. Samples were then run twice more through the flow cytometer at 30 min interval.

Statistical Analyses. All statistical analyses were performed in GraphPad Prism 8. For insertion site screening, the differences in cpGFP fluorescence between GR24 and control were tested using one sample *t* tests (two-tailed). To test responses to Triton X-100, data were compared using one-way analysis of variance (ANOVA). *Posthoc* Dunnett's multiple comparison tests were used to compare each treatment against the −Triton X-100 −GR24 control. For *in vitro* dose−response curves, GFP/LssmOrange fluorescence intensities were normalized to a scale of 0 to 100, and fit to an [agonist] *vs* response − variable slope (four parameters) model. Where EC50 values were compared, an extra sum-of-squares F test was used, with a *p*-value cutoff of 0.05. *In vivo* protoplast or yeast dose−response curves were fit to an [agonist] *vs* response − variable slope (four parameters) model.

■ ASSOCIATED CONTENT

Supporting Information

The Supporting Information is available free of charge at https://pubs.acs.org/doi/10.1021/acssynbio.0c00192.

> Expression and solubility of cpGFP-DAD2 and cpGFP-ShHTL7-LSSmOrange chimers; fluorescent response to the strigolactone analogue 10 μM rac-GR24 at different cpGFP insertion sites measured in intact *E. coli*; *rac*-GR24 dose−response using purified hexahistidine-tagged DAD2 cPGFP(G164); alternative biosensor design based on a yeast two-hybrid approach; purification of hexahistidine-tagged DAD2 and DAD2 cPGFP(G166) using immobilized metal affinity chromatography; fluorescent response of rDAD2 cPGFP-(G164) and rShHTL7 cPGFP(L166) to Triton X-100; statistical analyses; coding sequences used in this study; primers used in this study (PDF)

■ AUTHOR INFORMATION

Corresponding Author

Jason H. Whitfield − *Australian Institute for Bioengineering and Nanotechnology, The University of Queensland, St Lucia, Brisbane, QLD 4072, Australia; Synthetic Biology Future Science Platform, CSIRO, Dutton Park, QLD 4001, Australia;* orcid.org/0000-0001-5037-6389; Email: j.whitfield@uq.edu.au

Authors

Rebecca J. Chesterfield − *Australian Institute for Bioengineering and Nanotechnology, The University of Queensland, St Lucia, Brisbane, QLD 4072, Australia; Synthetic Biology Future Science Platform, CSIRO, Black Mountain, ACT 2601, Australia*

Benjamin Pouvreau − *Synthetic Biology Future Science Platform, CSIRO, Black Mountain, ACT 2601, Australia*

Da Cao − *School of Biological Sciences, The University of Queensland, St Lucia, Brisbane, QLD 4072, Australia*

Kirill Alexandrov − *Synthetic Biology Future Science Platform, CSIRO, Dutton Park, QLD 4001, Australia; CSIRO-QUT Synthetic Biology Alliance, ARC Centre of Excellence in Synthetic Biology, Centre for Agriculture and the Bioeconomy, Institute of Health and Biomedical Innovation, Institute for Future Environments, School of Biology and Environmental Science, Queensland University of Technology, Brisbane, QLD 4001, Australia*

Christine A. Beveridge − *School of Biological Sciences, The University of Queensland, St Lucia, Brisbane, QLD 4072, Australia*

Claudia E. Vickers − *Australian Institute for Bioengineering and Nanotechnology, The University of Queensland, St Lucia, Brisbane, QLD 4072, Australia; Synthetic Biology Future Science Platform, CSIRO, Dutton Park, QLD 4001, Australia*

Complete contact information is available at: https://pubs.acs.org/10.1021/acssynbio.0c00192

Author Contributions

R.J.C. designed and performed experiments and interpreted data. J.H.W. developed the biosensor designs and oversaw the study design. R.J.C. and J.H.W. wrote the manuscript. B.P. performed all protoplast experiments. D.C. developed methods for analysis of GR24 hydrolysis and did critical revision of the manuscript. C.A.B., C.E.V., and K.A critically reviewed the manuscript and advised on study design.

Notes

The authors declare no competing financial interest.

■ ACKNOWLEDGMENTS

The authors acknowledge the facilities, and the scientific and technical assistance of the School of Chemistry and Molecular Biosciences Mass Spectrometry Facility and The University of Queensland. We thank Christopher S. P. McErlean (The University of Sydney) and Gavin Flematti (University of Western Australia) for providing compounds used in this study. R.J.C. is funded by a CSIRO Synthetic Biology Future Science Platform PhD Top-Up Scholarship, and an Australian Government Research Training Program Stipend. J.H.W. is supported by a CSIRO Synthetic Biology Future Fellowship. B.P. was partly funded through the CSIRO Synthetic Biology Future Science Platform and the CSIRO Research Office CERC Postdoctoral Fellowship scheme. C.A.B. is funded by an ARC Georgina Sweet Laureate Fellowship FL180100139. K.A. gratefully acknowledges financial support of QUT/CSIRO Synthetic Biology alliance.

■ ABBREVIATIONS

SL, strigolactone; cpGFP, circularly permuted green fluorescent protein; Y2H, yeast two-hybrid; LSSmOrange, Long Stokes shift monomeric orange fluorescent protein; PDB, Protein Data Bank; yEGFP, yeast-enhanced green fluorescent protein; NAA, 1-naphthaleneacetic acid; GA3, gibberellic acid; BA, 6-benzylaminopurine.

REFERENCES

(1) Agusti, J. (2017) Strigolactone-mediated Stimulation of Secondary Xylem Proliferation in Stems. *Methods Mol. Biol. 1544*, 21−26.

(2) Gomez-Roldan, V., Fermas, S., Brewer, P. B., Puech-Pagès, V., Dun, E. A., Pillot, J.-P., Letisse, F., Matusova, R., Danoun, S., Portais, J.-C., et al. (2008) Strigolactone inhibition of shoot branching. *Nature 455*, 189−194.

(3) Kapulnik, Y., Delaux, P.-M., Resnick, N., Mayzlish-Gati, E., Wininger, S., Bhattacharya, C., Séjalon-Delmas, N., Combier, J.-P., Bécard, G., Belausov, E., et al. (2011) Strigolactones affect lateral root formation and root-hair elongation in Arabidopsis. *Planta 233*, 209−216.

(4) Rasmussen, A., Mason, M. G., De Cuyper, C., Brewer, P. B., Herold, S., Agusti, J., Geelen, D., Greb, T., Goormachtig, S., Beeckman, T., et al. (2012) Strigolactones suppress adventitious rooting in Arabidopsis and pea. *Plant Physiol. 158*, 1976−1987.

(5) Umehara, M., Hanada, A., Yoshida, S., Akiyama, K., Arite, T., Takeda-Kamiya, N., Magome, H., Kamiya, Y., Shirasu, K., Yoneyama, K., et al. (2008) Inhibition of shoot branching by new terpenoid plant hormones. *Nature 455*, 195−200.

(6) Yamada, Y., Furusawa, S., Nagasaka, S., Shimomura, K., Yamaguchi, S., and Umehara, M. (2014) Strigolactone signaling regulates rice leaf senescence in response to a phosphate deficiency. *Planta 240*, 399−408.

(7) Davidson, E. A., Bayer, T. S., Windram, O., and Hleba, Y. (2016) Strigolactone formulations and uses thereof. Eur. Pat. EP3060561A1.

(8) Van Ha, C., Leyva-González, M. A., Osakabe, Y., Tran, U. T., Nishiyama, R., Watanabe, Y., Tanaka, M., Seki, M., Yamaguchi, S., Van Dong, N., et al. (2014) Positive regulatory role of strigolactone in plant responses to drought and salt stress. *Proc. Natl. Acad. Sci. U. S. A. 111*, 851−856.

(9) Liu, J., He, H., Vitali, M., Visentin, I., Charnikhova, T., Haider, I., Schubert, A., Ruyter-Spira, C., Bouwmeester, H. J., Lovisolo, C., et al. (2015) Osmotic stress represses strigolactone biosynthesis in Lotus japonicus roots: exploring the interaction between strigolactones and ABA under abiotic stress. *Planta 241*, 1435−1451.

(10) Akiyama, K., Matsuzaki, K., and Hayashi, H. (2005) Plant sesquiterpenes induce hyphal branching in arbuscular mycorrhizal fungi. *Nature 435*, 824−827.

(11) Vurro, M., Boari, A., Thiombiano, B., and Bouwmeester, H. (2019) Strigolactones and Parasitic Plants, in *Strigolactones—Biology and Applications*, pp 89−120, Springer International Publishing, Cham.

(12) Parker, C. (2009) Observations on the current status of Orobanche and Striga problems worldwide. *Pest Manage. Sci. 65*, 453−459.

(13) Kgosi, R. L., Zwanenburg, B., Mwakaboko, A. S., and Murdoch, A. J. (2012) Strigolactone analogues induce suicidal seed germination of Striga spp. in soil. *Weed Res. 52*, 197−203.

(14) Samejima, H., Babiker, A. G., Takikawa, H., Sasaki, M., and Sugimoto, Y. (2016) Practicality of the suicidal germination approach for controlling Striga hermonthica. *Pest Manage. Sci. 72*, 2035−2042.

(15) Zwanenburg, B., Mwakaboko, A. S., and Kannan, C. (2016) Suicidal germination for parasitic weed control. *Pest Manage. Sci. 72*, 2016−2025.

(16) Vurro, M., Prandi, C., and Baroccio, F. (2016) Strigolactones: how far is their commercial use for agricultural purposes? *Pest Manage. Sci. 72*, 2026−2034.

(17) Gobena, D., Shimels, M., Rich, P. J., Ruyter-Spira, C., Bouwmeester, H., Kanuganti, S., Mengiste, T., and Ejeta, G. (2017) Mutation in sorghum LOW GERMINATION STIMULANT 1 alters strigolactones and causes Striga resistance. *Proc. Natl. Acad. Sci. U. S. A. 114*, 4471−4476.

(18) Dor, E., Yoneyama, K., Wininger, S., Kapulnik, Y., Yoneyama, K., Koltai, H., Xie, X., and Hershenhorn, J. (2011) Strigolactone deficiency confers resistance in tomato line SL-ORT1 to the parasitic weeds Phelipanche and Orobanche spp. *Phytopathology 101*, 213−22.

(19) Fernández-Aparicio, M., Kisugi, T., Xie, X., Rubiales, D., and Yoneyama, K. (2014) Low strigolactone root exudation: A novel mechanism of broomrape (Orobanche and Phelipanche spp.) resistance available for faba bean breeding. *J. Agric. Food Chem. 62*, 7063−7071.

(20) Pavan, S., Schiavulli, A., Marcotrigiano, A. R., Bardaro, N., Bracuto, V., Ricciardi, F., Charnikhova, T., Lotti, C., Bouwmeester, H., and Ricciardi, L. (2016) Characterization of Low-Strigolactone Germplasm in Pea (Pisum sativum L.) Resistant to Crenate Broomrape (Orobanche crenata Forsk.). *Mol. Plant-Microbe Interact. 29*, 743−749.

(21) Bürger, M., and Chory, J. (2020) The Many Models of Strigolactone Signaling. *Trends Plant Sci. 25*, 395−405.

(22) Jiang, L., Liu, X., Xiong, G., Liu, H., Chen, F., Wang, L., Meng, X., Liu, G., Yu, H., Yuan, Y., et al. (2013) DWARF 53 acts as a repressor of strigolactone signalling in rice. *Nature 504*, 401−405.

(23) Zhou, F., Lin, Q., Zhu, L., Ren, Y., Zhou, K., Shabek, N., Wu, F., Mao, H., Dong, W., Gan, L., Ma, W., Gao, H., Chen, J., Yang, C., Wang, D., Tan, J., Zhang, X., Guo, X., Wang, J. J., Jiang, L., Liu, X., Chen, W., Chu, J., Yan, C., Ueno, K., Ito, S., Asami, T., Cheng, Z., Wang, J. J., Lei, C., Zhai, H., Wu, C., Wang, H., Zheng, N., and Wan, J. (2013) D14-SCFD3-dependent degradation of D53 regulates strigolactone signalling. *Nature 504*, 406−410.

(24) Chevalier, F., Nieminen, K., Sánchez-Ferrero, J. C., Rodríguez, M. L., Chagoyen, M., Hardtke, C. S., and Cubas, P. (2014) Strigolactone promotes degradation of DWARF14, an α/β hydrolase essential for strigolactone signaling in Arabidopsis. *Plant Cell 26*, 1134−50.

(25) Hu, Q., He, Y., Wang, L., Liu, S., Meng, X., Liu, G., Jing, Y., Chen, M., Song, X., Jiang, L., Yu, H., Wang, B., and Li, J. (2017) DWARF14, a receptor covalently linked with the active form of strigolactones, undergoes strigolactone-dependent degradation in rice. *Front. Plant Sci.*, DOI: 10.3389/fpls.2017.01935.

(26) Yoneyama, K., Xie, X., Yoneyama, K., Kisugi, T., Nomura, T., Nakatani, Y., Akiyama, K., and McErlean, C. S. P. (2018) Which are the major players, canonical or non-canonical strigolactones? *J. Exp. Bot. 69*, 2231−2239.

(27) Yasui, R., Seto, Y., Ito, S., Kawada, K., Itto-Nakama, K., Mashiguchi, K., and Yamaguchi, S. (2019) Chemical screening of novel strigolactone agonists that specifically interact with DWARF14 protein. *Bioorg. Med. Chem. Lett. 29*, 938−942.

(28) Chesterfield, R. J., Vickers, C. E., and Beveridge, C. A. (2020) Translation of Strigolactones from Plant Hormone to Agriculture: Achievements, Future Perspectives, and Challenges. *Trends Plant Sci.*, DOI: 10.1016/j.tplants.2020.06.005.

(29) Samodelov, S. L., Beyer, H. M., Guo, X., Augustin, M., Jia, K.-P., Baz, L., Ebenhöh, O., Beyer, P., Weber, W., Al-Babili, S., et al. (2016) StrigoQuant: A genetically encoded biosensor for quantifying strigolactone activity and specificity. *Sci. Adv. 2*, No. e1601266.

(30) Sanchez, E., Artuso, E., Lombardi, C., Visentin, I., Lace, B., Saeed, W., Lolli, M. L., Kobauri, P., Ali, Z., Spyrakis, F., Cubas, P., Cardinale, F., and Prandi, C. (2018) Structure-activity relationships of strigolactones *via* a novel, quantitative in planta bioassay. *J. Exp. Bot. 69*, 2333−2343.

(31) Hamiaux, C., Drummond, R. S. M. S. M., Janssen, B. J. J., Ledger, S. E. E., Cooney, J. M. M., Newcomb, R. D. D., and Snowden, K. C. C. (2012) DAD2 is an α/β hydrolase likely to be involved in the perception of the plant branching hormone, strigolactone. *Curr. Biol. 22*, 2032−2036.

(32) Toh, S., Holbrook-Smith, D., Stokes, M. E. E., Tsuchiya, Y., and McCourt, P. (2014) Detection of parasitic plant suicide germination compounds using a high-throughput Arabidopsis HTL/KAI2 strigolactone perception system. *Chem. Biol. 21*, 988−998.

(33) Tamura, T., and Hamachi, I. (2014) Recent Progress in Design of Protein-Based Fluorescent Biosensors and Their Cellular Applications. *ACS Chem. Biol. 9*, 2708−2717.

(34) Nadler, D. C., Morgan, S.-A., Flamholz, A., Kortright, K. E., and Savage, D. F. (2016) Rapid construction of metabolite biosensors using domain-insertion profiling. *Nat. Commun. 7*, 12266.

(35) Ostermeier, M. (2005) Engineering allosteric protein switches by domain insertion. *Protein Eng., Des. Sel. 18*, 359−364.
(36) Marvin, J. S., Schreiter, E. R., Echevarría, I. M., and Looger, L. L. (2011) A genetically encoded, high-signal-to-noise maltose sensor. *Proteins: Struct., Funct., Genet. 79*, 3025−3036.
(37) Hu, H., Gu, Y., Xu, L., Zou, Y., Wang, A., Tao, R., Chen, X., Zhao, Y., and Yang, Y. (2017) A genetically encoded toolkit for tracking live-cell histidine dynamics in space and time. *Sci. Rep. 7*, 43479.
(38) Kostyuk, A. I., Demidovich, A. D., Kotova, D. A., Belousov, V. V., and Bilan, D. S. (2019) Circularly permuted fluorescent protein-based indicators: History, principles, and classification. *Int. J. Mol. Sci. 20*, 4200.
(39) Baird, G. S., Zacharias, D. A., and Tsien, R. Y. (1999) Circular permutation and receptor insertion within green fluorescent proteins. *Proc. Natl. Acad. Sci. U. S. A. 96*, 11241−11246.
(40) Yao, R., Ming, Z., Yan, L., Li, S., Wang, F., Ma, S., Yu, C., Yang, M., Chen, L., Chen, L., Li, Y., Yan, C., Miao, D., Sun, Z., Yan, J., Sun, Y., Wang, L., Chu, J., Fan, S., He, W., Deng, H., Nan, F., Li, J., Rao, Z., Lou, Z., and Xie, D. (2016) DWARF14 is a non-canonical hormone receptor for strigolactone. *Nature 536*, 469−473.
(41) Zhao, L.-H., Zhou, X. E., Wu, Z.-S., Yi, W., Xu, Y. Y., Li, S., Xu, T.-H., Liu, Y., Chen, R.-Z., Kovach, A., Kang, Y., Hou, L., He, Y., Xie, C., Song, W., Zhong, D., Xu, Y. Y., Wang, Y., Li, J., Zhang, C., Melcher, K., and Xu, H. E. (2013) Crystal structures of two phytohormone signal-transducing α/β hydrolases: karrikin-signaling KAI2 and strigolactone-signaling DWARF14. *Cell Res. 23*, 436−439.
(42) Marvin, J. S., Borghuis, B. G., Tian, L., Cichon, J., Harnett, M. T., Akerboom, J., Gordus, A., Renninger, S. L., Chen, T. W., Bargmann, C. I., Orger, M. B., Schreiter, E. R., Demb, J. B., Gan, W. B., Hires, S. A., and Looger, L. L. (2013) An optimized fluorescent probe for visualizing glutamate neurotransmission. *Nat. Methods 10*, 162−170.
(43) Carlsson, G. H., Hasse, D., Cardinale, F., Prandi, C., and Andersson, I. (2018) The elusive ligand complexes of the DWARF14 strigolactone receptor. *J. Exp. Bot. 69*, 2345−2354.
(44) Seto, Y., Yasui, R., Kameoka, H., Tamiru, M., Cao, M., Terauchi, R., Sakurada, A., Hirano, R., Kisugi, T., Hanada, A., Umehara, M., Seo, E., Akiyama, K., Burke, J., Takeda-Kamiya, N., Li, W., Hirano, Y., Hakoshima, T., Mashiguchi, K., Noel, J. P., Kyozuka, J., and Yamaguchi, S. (2019) Strigolactone perception and deactivation by a hydrolase receptor DWARF14. *Nat. Commun. 10*, 191.
(45) de Saint Germain, A., Clavé, G., Badet-Denisot, M.-A., Pillot, J.-P., Cornu, D., Le Caer, J.-P., Burger, M., Pelissier, F., Retailleau, P., Turnbull, C., Bonhomme, S., Chory, J., Rameau, C., and Boyer, F.-D. (2016) An histidine covalent receptor and butenolide complex mediates strigolactone perception. *Nat. Chem. Biol. 12*, 787−794.
(46) Yao, R., Wang, F., Ming, Z., Du, X., Chen, L., Wang, Y., Zhang, W., Deng, H., and Xie, D. (2017) ShHTL7 is a non-canonical receptor for strigolactones in root parasitic weeds. *Cell Res. 27*, 838−841.
(47) Yao, R., Wang, L., Li, Y., Chen, L., Li, S., Du, X., Wang, B., Yan, J., Li, J., and Xie, D. (2018) Rice DWARF14 Acts as an Unconventional Hormone Receptor for Strigolactone. *J. Exp. Bot. 69*, 2355.
(48) Ast, C., Foret, J., Oltrogge, L. M., De Michele, R., Kleist, T. J., Ho, C.-H., and Frommer, W. B. (2017) Ratiometric Matryoshka biosensors from a nested cassette of green- and orange-emitting fluorescent proteins. *Nat. Commun. 8*, 431.
(49) Boutet-Mercey, S., Perreau, F., Roux, A., Clavé, G., Pillot, J.-P., Schmitz-Afonso, I., Touboul, D., Mouille, G., Rameau, C., and Boyer, F.-D. (2018) Validated Method for Strigolactone Quantification by Ultra High-Performance Liquid Chromatography - Electrospray Ionisation Tandem Mass Spectrometry Using Novel Deuterium Labelled Standards. *Phytochem. Anal. 29*, 59.
(50) Wang, L., Wang, B., Jiang, L., Liu, X., Li, X., Lu, Z., Meng, X., Wang, Y., Smith, S. M., and Li, J. (2015) Strigolactone signaling in Arabidopsis regulates shoot development by targeting D53-like SMXL repressor proteins for ubiquitination and degradation. *Plant Cell 27*, 3128−3142.
(51) Zhao, J., Wang, T., Wang, M., Liu, Y., Yuan, S., Gao, Y., Yin, L., Sun, W., Peng, L., Zhang, W., Wan, J., and Li, X. (2014) DWARF3 participates in an SCF complex and associates with DWARF14 to suppress rice shoot branching. *Plant Cell Physiol. 55*, 1096−1109.
(52) Song, X., Lu, Z., Yu, H., Shao, G., Xiong, J., Meng, X., Jing, Y., Liu, G., Xiong, G., Duan, J., Yao, X.-F., Liu, C.-M., Li, H., Wang, Y., and Li, J. (2017) IPA1 functions as a downstream transcription factor repressed by D53 in strigolactone signaling in rice. *Cell Res. 27*, 1128−1141.
(53) Lumba, S., Holbrook-Smith, D., and McCourt, P. (2017) The perception of strigolactones in vascular plants. *Nat. Chem. Biol. 13*, 599−606.
(54) Conn, C. E., Bythell-Douglas, R., Neumann, D., Yoshida, S., Whittington, B., Westwood, J. H., Shirasu, K., Bond, C. S., Dyer, K. A., and Nelson, D. C. (2015) Convergent evolution of strigolactone perception enabled host detection in parasitic plants. *Science 349*, 540−3.
(55) Shahul Hameed, U., Haider, I., Jamil, M., Kountche, B. A., Guo, X., Zarban, R. A., Kim, D., Al-Babili, S., and Arold, S. T. (2018) Structural basis for specific inhibition of the highly sensitive ShHTL7 receptor. *EMBO Rep. 19*, No. e45619.
(56) Xu, Y., Miyakawa, T., Nosaki, S., Nakamura, A., Lyu, Y., Nakamura, H., Ohto, U., Ishida, H., Shimizu, T., Asami, T., and Tanokura, M. (2018) Structural analysis of HTL and D14 proteins reveals the basis for ligand selectivity in Striga. *Nat. Commun. 9*, 3947.
(57) Tullman, J., Nicholes, N., Dumont, M. R., Ribeiro, L. F., and Ostermeier, M. (2016) Enzymatic protein switches built from paralogous input domains. *Biotechnol. Bioeng. 113*, 852−858.
(58) Uraguchi, D., Kuwata, K., Hijikata, Y., Yamaguchi, R., Imaizumi, H., AM, S., Rakers, C., Mori, N., Akiyama, K., Irle, S., McCourt, P., Kinoshita, T., Ooi, T., and Tsuchiya, Y. (2018) A femtomolar-range suicide germination stimulant for the parasitic plant. *Science (Washington, DC, U. S.) 362*, 1301−1305.
(59) Pouvreau, B., Blundell, C., Vohra, H., Zwart, A. B., Arndell, T., Singh, S., and Vanhercke, T. (2020) A Versatile High Throughput Screening Platform for Plant Metabolic Engineering Highlights the Major Role of ABI3 in Lipid Metabolism Regulation. *Front. Plant Sci.*, DOI: 10.3389/fpls.2020.00288.